The 4th European sCO2 Conference for Energy Systems
March 23-24, 2021, Online Conference

2021-sCO2.eu-154

EXERGOECONOMIC ANALYSIS OF A HYBRID sCO2 BRAYTON POWER CYCLE

Abdurrahman Alenezi*
University of Central Florida
Orlando, USA
Email: aaalenezi@knights.ucf.edu

Ladislav Vesely
University of Central Florida
Orlando, USA

Jayanta Kapat
University of Central Florida
Orlando, USA

ABSTRACT

An exergoeconomic analysis of a hybrid power generation cycle is performed on its standalone constituents. The hybrid is based on Allam cycle configuration. Allam cycle is a supercritical carbon dioxide oxy-combustion (OC) Brayton cycle. The proposed hybrid utilizes solar power as its primary heat source and natural gas OC as a complementing heat source. The purpose of the complimenting heat source is to make up for the lost time when the sun is not available due to bad weather conditions or at nighttime. This is done to ensure the reliability, responsiveness, and availability of the cycle for power generation at all times. The hybrid is an attempt to provide power with minimal adverse effects on the environment. This study is divided into three major steps. The first and second are energy and exergy analysis. The third step is exergoeconomic analysis to obtain the cost contribution of each component relative to the cycle's final product. Although both configurations brought similar power output and second law efficiency, the energy efficiency was higher for the OC configuration. The total product cost ($/GJ) for the OC configuration was half of that for the concentrated solar power (CSP). The unit cost of electricity in (Cent/kWh) for the CSP standalone configuration is approximately 60% higher than that of the OC configuration. In the CSP configuration, the main heat exchanger and the recuperator are the most critical units to consider for savings. Therefore, reducing the exergy destruction in the CSP main heat exchanger and the recuperator units could be cost-effective for the entire cycle, even if this would increase the component investment costs. Therefore, for exergoeconomic performance enhancement, using a recuperator with higher efficiency is recommended. On the other hand, the combustor and air separation unit (ASU) are the most critical units to consider for savings for the OC configuration. Therefore, a replacement for the ASU unit with a lower purchasing cost is recommended for overall exergoeconomic performance enhancement. The parametric study results showed that increasing the turbine's inlet temperature is conducive to improving both configurations' thermodynamic and exergoeconomic performances. Similar trends were also obtained for the turbine inlet pressure for both configurations.

INTRODUCTION

Energy production and consumption are forecasted to increase for the foreseeable future due to population growth and higher living standards. Electricity production is projected to stay the primary type of energy demand globally up to 2050 [1].

Thermal power cycles converting thermal energy to electricity is the leading technology used to generate electricity [1]. Although various combustion technologies are utilized to convert fossil fuels to thermal energy to act as the heat source for thermal power cycles, this process's byproducts usually pollute the environment. Combustion of fossil fuels produces greenhouse gases (GHG), which is the main contributor to global warming. A good solution to this problem is to improve the existing power generation technologies efficiency, develop new clean technologies, or combine compatible technologies to produce more efficient hybrid cycles.

Compared to traditional power cycles, supercritical carbon dioxide (sCO_2) Brayton power cycles are promising because they have higher efficiency, smaller equipment size, and better economics. The cycle's higher efficiency is mainly due to its recuperative nature. Additionally, the critical point of CO_2 is near the surroundings temperature, which means that exergy losses due to temperature differences with the environment are minimal. Another good quality of this cycle is the high density of CO_2 near its critical point, which results in less work at the compressor. Furthermore, the sCO_2 power cycle can work with direct and indirect heat sources because it can accept a wide range of heat sources. This advantage allows it to work with high-temperature heat sources such as nuclear [2] and low-temperature heat sources such as waste heat [3].

* corresponding author(s)

DOI: 10.17185/duepublico/73980

Nevertheless, the sCO_2 cycle has some disadvantages as operating near CO_2 critical point brings its own challenges. Since CO_2 properties vary significantly near its critical point, a few degrees change in its temperature may substantially affect the cycle's operations and control. Therefore, keeping the cycle at its optimum operating conditions is difficult as small fluctuations in CO_2 properties can negatively affect its efficiency [4].

A good enhancement of Brayton power cycle is the use of OC technology. Oxy-combustion is a process in which fuel is combusted in an oxygen-rich environment instead of air. The combustion products, in this case, are mainly CO_2 and water (H_2O). Allam cycle is an OC cycle based on Brayton power cycle configuration. Allam cycle fuel feed is natural gas (NG), or synthetic gas produced from coal [5]. Allam cycle is considered semi-closed as it takes oxygen and fuel as its feed and rejects part of its produced CO_2 and water. Typically, an OC cycle uses an ASU to separate its air intake into Nitrogen (N_2), Oxygen (O_2), and Argon (Ar). The ASU outlet separation percentages are approximately 78.09%, 20.95% and 0.93% for N_2, O_2 and Ar, respectively [6]. Cryogenic air separation technology is the most common technology used for air separation.

In contrast to combustion utilizing air, OC avoids producing Nitrous Oxides (NO_x) by excluding N_2 from its combustor feed. OC is considered among the carbon capture technologies as it inhibits the release of CO_2 into the atmosphere by capturing it as part of its built-in technology [7]. The cycle also provides its export CO_2 in pure form and highly pressured, making it ideal for storage or export to other industries such as enhanced oil recovery. Since the withdrawn CO_2 is pure and pressurized, there is no need for additional physical or chemical processes prior to its export [8]. Hence, the pollution treatment cost is eliminated in this case. Another advantage of Allam cycle is that it can be heated directly and indirectly. A good example of direct heat addition is combustion, while an indirect heat addition can be, for example, solar power or waste heat.

There are several OC cycles; however, Allam cycle is considered one of the best. Barbra et al [9] performed a study on nineteen different OC power cycle configurations and concluded that Allam cycle configuration is the best for NG powered cycles. Allam cycle has higher efficiency compared to traditional Brayton power cycles. In a study by Allam et al, the authors claimed an overall cycle efficiency of 59% [10].

Another good strategy to avoid pollution from the power industry is to utilize renewable energy resources. The main categories of energy resources remain renewable, nuclear, and fossil fuels [11]. However, out of the three categories, renewable energy is the cleanest from the environmental perspective. Renewable energy resources comprise solar, wind, geothermal, hydropower, and biomass [12].

One of the most promising technologies in solar power is the CSP technology. In a typical CSP setup, solar radiation is focused using reflective surfaces against solar collectors [13]. A solar collector's job is to transform the collected solar radiation into thermal energy. Afterward, the converted thermal energy is used to heat the heat transfer fluid (HTF), such as molten salt. The heat accumulated within the HTF is then transferred to the power generation cycle working fluid via a special heat exchanger. However, due to bad weather conditions and during nighttime, the sun is not always shining. Due to fluctuations in its thermal energy, most CSP systems have thermal storage vessels to store their HTF. The storage vessels' purpose is to provide a consistent quality stream to the heat exchanger and within the required operating conditions. One of the leading CSP technologies is the solar tower technology. Temperatures in a solar tower can reach an operating temperature between 300 ^oC and 1500 ^oC [14].

From a thermodynamic perspective, to achieve a higher thermal-to-electric conversion efficiency, higher operating temperatures are desirable [15]. Fossil fuel and nuclear power cycles have similar thermodynamics to the CSP cycles. However, nuclear and CSP cycles heat addition to the cycle is in the form of heat flux while fossil fuel heat is sensible heat [16].

Hybrid cycles are those combining more than one technology to produce an enhanced cycle with better outcomes. The combination of renewable and traditional fossil fuel cycles is an example of such hybrid cycles. In addition to better economics, hybrid cycles are generally more reliable than sole renewable energy cycles and usually have higher efficiency. For example, a study [17] evaluated hybridizing between conventional and standalone renewable power cycles. The study concluded that hybrid plants could save up to 50% compared to standalone ones.

This study carries out an exergoeconomic evaluation of a hybrid power cycle. The cycle is based on a simple recuperative Brayton cycle configuration with sCO_2 as its working fluid. The proposed cycle main processes are similar except for their heat source. The proposed cycle's primary heat source is CSP. However, CSP is complemented with natural gas OC to avoid solar energy discrepancy when the sun is not available. This combination is sought to provide better responsiveness to electrical grid demand fluctuations and add additional reliability to the cycle.

HYBRID CYCLE DESCRIPTION

As shown in Figure 1, the hybrid is simple recuperative based on Allam cycle configuration with two heat sources, solar and fossil fuel oxy-combustion. The solar power is provided by the CSP solar tower technology. The CSP heat source is the primary heat source; however, the OC heat source is utilized to complement the power generation requirements or act as a standalone in bad weather cases or at nighttime.

A conservation strategy was adopted in constructing the hybrid. Therefore, most of the hybrid equipment were made common for both configurations. The thinking behind this strategy of having the highest possible number of common equipment is to minimize cost both in terms of capital and operational costs. The common and unique units of the proposed hybrid cycle are shown in Table 1.

When the CSP heat source solely heats the hybrid as a standalone, the CSP main heat exchanger is exclusively providing 100% of the heat to the hybrid. The CSP main heat exchanger transfers heat between the HTF, molten salt, and the

power cycle working fluid, sCO_2. On the other hand, when the hybrid is solely heated by OC as a standalone, the NG combustor provides heat to the hybrid.

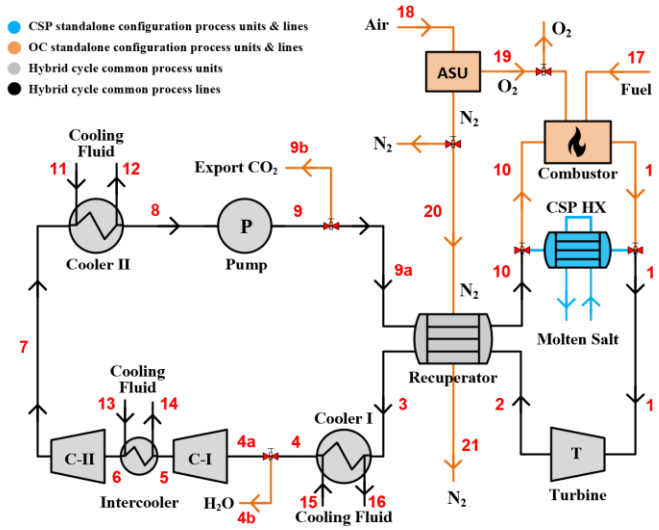

Figure 1: Schematic of the hybrid cycle

The CSP standalone configuration is a closed system. Furthermore, the OC standalone configuration is a semi-closed system where oxygen and NG are feed into the combustor, and water and export CO_2 are withdrawn out of the cycle. It is worth mentioning that the nitrogen stream coming from the ASU only contributes to heat transfer in the hybrid's recuperator and has no mass interactions within the cycle.

Table 1: Hybrid cycle common and unique units

Hybrid Cycle Unit	Unique/Common
Turbine (Turb)	Common
Compressors (C)	Common
CO_2 export pump (Pump)	Common
Coolers (Cl)	Common
Recuperator (Rec)	Common
CSP heat exchanger (CSP HX)	Unique to CSP configuration
Combustor (Comb)	Unique to OC configuration
ASU	Unique to OC configuration
Water separator (WS)	Unique to OC configuration

HYBRID CYCLE PROCESS

After gaining heat at the heat source, the high pressure and temperature working fluid at process point 1 is expanded in the turbine to produce work. The expanded working fluid at low pressure and high temperature at process point 2 then enters the recuperator's hot-stream side, where it cools down to process point 3. To prepare the working fluid to enter the compressor, it is further cooled down at cooler I. At this point, the process is at point 4. Then, CO_2 is compressed in compressors I and II and cooled in-between at the compressor's intercooler. The high pressure CO_2 at process point 7 is then cooled at cooler II to arrive at process point 8 before raising its pressure at the cycle's pump. The high pressure CO_2 at process point 9 enters the recuperator's cold-side to raise its temperature before returning to the heat source again at process point 10.

It is worth mentioning that in the CSP standalone case, the working fluid is pure CO_2. However, in the OC standalone case, pure CO_2 is only present between process points 4a and 10, while between process points 1 and 4a, the working fluid is a mixture of water and CO_2. The water is withdrawn out of the cycle in the water separator between process points 4 and 4a. In both configurations, the working fluid is assumed either pure CO_2 or a mixture of pure CO_2 and water with no impurities throughout the whole cycle.

HYBRID CYCLE MODELING

This study is divided into three parts: (1) energy, (2) exergy, and (3) exergoeconomic analyses. For each of the three parts, the study is conducted for both configurations as a standalone case each. The mass flow rate into the turbine inlet at process point 1 is constant at 125 Kg/s for both standalone cases. The process schematics of the proposed hybrid cycle for both standalone configurations are shown in Figures 2 and 3, showing all process streams. The P-h diagrams of the two standalone configurations are in Figures 4 and 5 in Annex A.

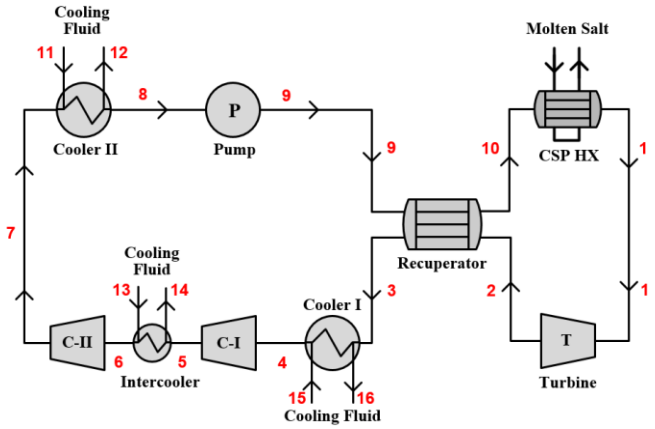

Figure 2: Schematic of the CSP standalone configuration

In addition to the aforementioned assumptions and constraints, the following are this study's main assumptions:

- All processes are under steady-state conditions.
- System heat losses to the environment are negligible.
- Potential and kinetic energy changes are negligible.
- The combustion process is complete.
- Combustion process flue gases are only H_2O and CO_2.
- Environmental ambient conditions are 25 ^oC and 1 atm.
- Turbine, compressors, and pumps assigned mean value isentropic efficiencies.
- Pressure drop is negligible for all equipment except for heat exchangers.
- The pressure drop for heat exchangers is 2%.

- A pinch point is assigned for all heat exchangers.
- Cooling water to coolers and intercooler is supplied at the dead state.

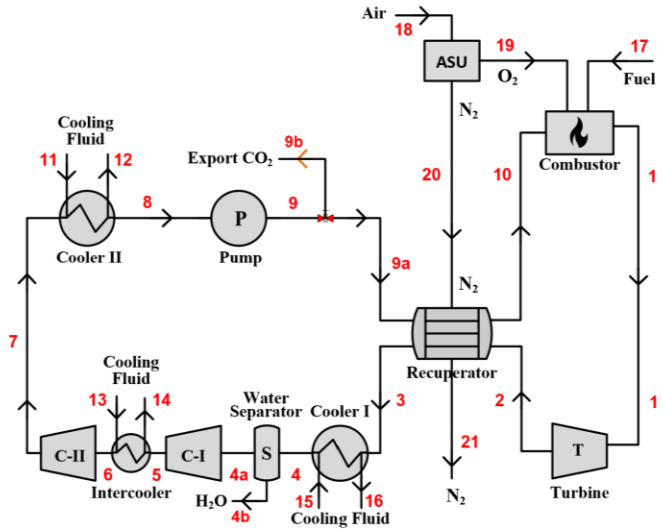

Figure 3: Schematic of the OC standalone configuration

All calculations and analyses are executed for the two cycle configurations, each as a standalone. Therefore, the analysis for each case is done separately and independently of the other configuration.

A. ENERGY ANALYSIS

The energy analysis for the cycle is based on the first law of thermodynamics. Hence, for each hybrid cycle unit, energy and mass conservation laws are applied for both cycle standalone configurations.

The input parameters in collaboration with model assumptions are inputs to the system model. Going through the major cycle units, a set of equations is developed for each unit until the whole cycle is covered.

System parameters of each unit are utilized to complete a set of equations for the system. For example, an isentropic efficiency value and its definition are utilized for the cases of pumps, compressors, and turbines, while pinch point temperature and effectiveness are utilized for a heat exchanger. Upon completing the set of equations for the system, a code is developed in Engineering Equation Solver (EES) software to solve the model and obtain its unknowns. System unknown variables are mainly the thermodynamic state properties of each unit. Upon obtaining all cycle unknowns, specific work for pumps, compressors, and turbines is obtained by applying the pertaining equation for each unit. A similar procedure also applies for calculating heat loads for the cycle's heat exchangers. At the end, the cycle's specific power output and the first law of thermodynamics efficiency for each case are determined. The ASU power consumption is not considered for the cycle's first law of thermodynamics efficiency and net power calculations. This part of the study is based on previous work published by this study's authors [18]. Model validation was also conducted in [18] and found satisfactory against published literature in this regard. However, some of the model's parameters were modified to represent the current study. Tables 2 and 3 present the model's temperature and mass flow rate of the energy analysis.

Table 2: Temperatures at the hybrid's main process points

Process Point	Temperature (°C)	
	CSP Configuration	OC Configuration
1	700	700
2	419.1	419.1
3	85.9	80.2
4	20	20
7	61.3	61.3
8	20	20
9	45.8	46.1
10	246.4	338.6

The previous study results showed that the CSP configuration's mass flow rate is constant at 125 kg/s but between 125 and 116 kg/s for the OC configuration. The mass flow rates of the main process points for both configurations are shown in Table 3.

Table 3: Mass flow rates at the hybrid's main process points

Process Point	Mass flowrate (kg/s)	
	CSP Configuration	OC Configuration
1, 2, 3	125	125
4, 5, 6, 7, 8	125	122.1
9, 10	125	116

B. EXERGY ANALYSIS

The exergy analysis model is established based on the second law of thermodynamics. The purpose of the exergy model is to assign energy losses within the hybrid cycle and quantify them. To obtain exergy of a system, the general exergy rate balance for an open system under steady-state conditions is used:

$$\sum_j \left(1 - \frac{T_o}{T_j}\right) \dot{Q}_i + \sum_i \dot{E}_i = \sum_e \dot{E}_e + \dot{W} + \dot{E}_D \qquad (1)$$

Where the term $\dot{Q}_i$ and $\dot{W}$ represents heat transfer and work, respectively. The terms E_i and E_e in the above equation are the collective representation of potential, kinetic, physical, and chemical exergy transfer of the inlets and outlets of the system [19] and $\dot{E}_D$ represents the systems exergy destruction. The subscripts "i" and "e" represent the inlets and outlets for each cycle unit while the subscript "j" represents the unit's heat sources. Under steady-state conditions, the exergy destruction in (kW) can be obtained from the below exergy rate balance for any unit in the CSP and OC configurations [20]:

$$\dot{E}_D = \sum_i \dot{m}_i e_i - \sum_e \dot{m}_e e_e + \sum_j \left(1 - \frac{T_o}{T_j}\right) \dot{Q}_i - \dot{W} \qquad (2)$$

Due to limited changes in their energy, the potential and kinetic energy terms are neglected as per the assumption made earlier. Therefore, at a given state, the specific exergy of a particular stream is calculated as the sum of its physical and chemical exergies as per the following equation [20]:

$$e = (h - h_o) - T_o(s - s_o) + \sum_{m=1}^{n} y_m(\mu_m^* - \mu_m^0) \qquad (3)$$

Where h, T, s, μ, and y are the specific enthalpy, temperature, specific entropy, chemical potential, and mass fraction, respectively. The superscript (*) represents the initial concentration at ambient temperature and pressure, while the super and subscript (o) represents dead states. Finally, the subscript "m" represents an individual substance in a mixture stream.

The standalone CSP configuration is assumed to have a constant chemical composition, and hence chemical exergy is not present for this configuration calculations. On the other side, the OC standalone configuration has variable chemical compositions in the fuel-O_2 mixture combustion, and therefore, chemical exergy is present in its calculations. As discussed earlier, for the OC standalone configuration, the combustor flue gases are mainly CO_2 and steam up until the water content is cooled in cooler I and then separated at the water separator before reaching point 4a of the process. Therefore, the stream composition from process points 1 to point 3 is water and CO_2, but between process points 4a and 10, the working fluid consists of pure CO_2.

The exergy supplied to the CSP main heat exchanger is calculated for the CSP configuration as input heat. For the OC configuration, the combustor fuel exergy is calculated based on the equations provided in [20]. The fuel exergy for the CSP and OC configurations are calculated as follows, respectively:

$$\dot{E}_{Fuel,CSP} = \left(1 - \frac{T_o}{T_s}\right)\dot{Q}_{CSP} \qquad (4)$$

$$\dot{E}_{Fuel,OC} = \dot{m}_{CH_4}\left[(h_{17} - h_{o,CH_4}) - T_o(s_{17} - s_{o,CH_4}) + \frac{824.348}{MW_{CH_4}}\right] \qquad (5)$$

Where $\dot{Q}_{CSP}$ is the heat supplied by molten salt to the CSP main heat exchanger, T_s and T_0 are the heat source temperature supplied from the solar tower's storage tank and dead state temperatures, respectively. MW_{CH_4} is the molecular weight of natural gas.

The exergy destruction of all hybrid cycle units and the fuel and products' exergies are shown in Table 4 for the CSP standalone configuration and in Table 5 for the OC standalone configuration.

The second law of thermodynamics exergy efficiency for each component is calculated as:

$$\epsilon_k = \frac{\dot{E}_{Product,k}}{\dot{E}_{Fuel,k}} \qquad (6)$$

Where $\dot{E}_{product,k}$ and $\dot{E}_{Fuel,k}$ are exergy of the product and fuel for the k[th] component, respectively.

Table 4: Fuel exergy, product exergy, and exergy destruction for the CSP standalone configuration

Unit	Fuel Exergy ($\dot{E}_{Fuel}$)	Product Exergy ($\dot{E}_{Product}$)	Exergy Destruction ($\dot{E}_D = \dot{E}_{Fuel} - \dot{E}_{Product}$)
CSP HX	$\dot{E}_{Fuel} + \dot{E}_{10}$	$\dot{E}_1$	$\dot{E}_{Fuel} - (\dot{E}_1 - \dot{E}_{10})$
Turb	$\dot{E}_2 - \dot{E}_1$	$\dot{W}_{turb}$	$(\dot{E}_2 - \dot{E}_1) - \dot{W}_{turb}$
Rec	$\dot{E}_2 - \dot{E}_3$	$\dot{E}_{10} - \dot{E}_9$	$(\dot{E}_2 - \dot{E}_3) - (\dot{E}_{10} - \dot{E}_9)$
Cl-I	$\dot{E}_{15} - \dot{E}_{16}$	$\dot{E}_4 - \dot{E}_3$	$(\dot{E}_{15} - \dot{E}_{16}) - (\dot{E}_4 - \dot{E}_3)$
C-I	$\dot{W}_{comp\ I}$	$\dot{E}_5 - \dot{E}_4$	$\dot{W}_{comp\ I} - (\dot{E}_5 - \dot{E}_4)$
IC	$\dot{E}_{13} - \dot{E}_{14}$	$\dot{E}_6 - \dot{E}_5$	$(\dot{E}_{13} - \dot{E}_{14}) - (\dot{E}_6 - \dot{E}_5)$
C-II	$\dot{W}_{comp\ II}$	$\dot{E}_7 - \dot{E}_6$	$\dot{W}_{comp\ II} - (\dot{E}_7 - \dot{E}_6)$
Cl-II	$\dot{E}_{11} - \dot{E}_{12}$	$\dot{E}_8 - \dot{E}_7$	$(\dot{E}_{11} - \dot{E}_{12}) - (\dot{E}_8 - \dot{E}_7)$
Pump	$\dot{W}_{pump}$	$\dot{E}_9 - \dot{E}_8$	$\dot{W}_{pump} - (\dot{E}_9 - \dot{E}_8)$

Table 5: Fuel exergy, product exergy, and exergy destruction for the OC standalone configuration

Unit	Fuel Exergy ($\dot{E}_{Fuel}$)	Product Exergy ($\dot{E}_{Product}$)	Exergy Destruction ($\dot{E}_D = \dot{E}_{Fuel} - \dot{E}_{Product}$)
ASU	$\dot{E}_{18} + \dot{W}_{ASU}$	$\dot{E}_{19} + \dot{E}_{20}$	$(\dot{E}_{18} + \dot{W}_{ASU}) - (\dot{E}_{19} + \dot{E}_{20})$
Comb	$\dot{E}_{17} + \dot{E}_{19} + \dot{E}_{10}$	$\dot{E}_1$	$\dot{E}_{17} + \dot{E}_{19} + \dot{E}_{10} - \dot{E}_1$
Turb	$\dot{E}_2 - \dot{E}_1$	$\dot{W}_{turb}$	$(\dot{E}_2 - \dot{E}_1) - \dot{W}_{turb}$
Rec	$\dot{E}_2 - \dot{E}_3$	$\dot{E}_{10} - \dot{E}_{9a}$	$(\dot{E}_2 - \dot{E}_3) - (\dot{E}_{10} - \dot{E}_{9a})$
Cl-I	$\dot{E}_{15} - \dot{E}_{16}$	$\dot{E}_4 - \dot{E}_3$	$(\dot{E}_{15} - \dot{E}_{16}) - (\dot{E}_4 - \dot{E}_3)$
C-I	$\dot{W}_{comp\ I}$	$\dot{E}_5 - \dot{E}_{4a}$	$\dot{W}_{comp\ I} - (\dot{E}_5 - \dot{E}_{4a})$
IC	$\dot{E}_{13} - \dot{E}_{14}$	$\dot{E}_6 - \dot{E}_5$	$(\dot{E}_{13} - \dot{E}_{14}) - (\dot{E}_6 - \dot{E}_5)$
C-II	$\dot{W}_{comp\ II}$	$\dot{E}_7 - \dot{E}_6$	$\dot{W}_{comp\ II} - (\dot{E}_7 - \dot{E}_6)$
Cl-II	$\dot{E}_{11} - \dot{E}_{12}$	$\dot{E}_8 - \dot{E}_7$	$(\dot{E}_{11} - \dot{E}_{12}) - (\dot{E}_8 - \dot{E}_7)$
Pump	$\dot{W}_{pump}$	$\dot{E}_9 - \dot{E}_8$	$\dot{W}_{pump} - (\dot{E}_9 - \dot{E}_8)$

C. EXERGOECONOMIC ANALYSIS

The exergoeconomic analysis involves both exergy and economic inputs for each of the cycle unit. The exergoeconomic analysis can, in due course, be used as a tool to optimize the system's cost as the analysis goes through each unit and stream of the cycle. By the end of the exergoeconomic analysis, each of the cycle units and streams' contribution to the final product's cost is quantified. Note that the main final product of the hybrid cycle under this study is power production.

Assuming a cycle unit that receives heat and generates work, the following general cost rate balance equation is applied to its inlet and outlet streams [20]:

$$\dot{C}_{q,k} + \sum_i \dot{C}_{i,k} + \dot{Z}_k = \sum_e \dot{C}_{e,k} + \dot{C}_{w,k} \qquad (7)$$

Where $\dot{C}_{q,k}$ is the cost rate associated with thermal energy, $\dot{C}_{i,k}$ and $\dot{C}_{e,k}$ are the cost rates associated with the inlet and outlet streams of a cycle unit, respectively and $\dot{C}_{w,k}$ is the cost rate associated with power. All previous cost rates are in units of $(\$/hr)$. The above equation states that, for a unit or a system, the total cost of exergy of exiting streams is equal to the total spending to acquire them. In other words, the cost rate of a product is equal to the overall rate of spending utilized to generate that product. The cost per unit exergy (c) of a cycle unit in ($/GJ) is calculated by dividing the stream's exergy cost rate $\dot{C}$ by its exergy $\dot{E}$ as per the following relationship:

$$\mathrm{c}_k\ (\$/GJ) = \left(\frac{\dot{C}_k}{\dot{E}_k}\right) \qquad (8)$$

Evaluating the cost of a power cycle involves accounting for capital, operating, and maintenance charges expended to produce the cycle's product. Capital costs account for expenses related to plant construction and purchase values of its equipment [21] while operating and maintenance costs represent expenses related to power, raw materials, fuel, manpower, ...etc. During the lifetime of a plant, the cost of a particular resource or commodity, such as fuel, usually varies from one point in time to another. Therefore, levelized costs are utilized in assessing the cycle under study [22].

The capital, operational, and maintenance costs are accounted for by the following equation [20, 23]:

$$\dot{Z}_k\ (\$/h) = (Z_k\ .CRF)\left(\frac{\varphi}{\tau}\right) \qquad (9)$$

Where φ is the plant maintenance factor, and τ is the annual operational availability of the plant in $(hr/year)$. For the purpose of this study, the plant maintenance factor is assumed 1.06, and the annual availability of the plant for operations is assumed 8,000 hours per year [24]. The acronym *CRF* in the above equation is the capital recovery factor. The value of *CRF* accounts for three kinds of costs; the hourly capital investment cost, the operational cost, and maintenance cost. *CRF* is calculated by the following equation [20]:

$$CRF\ = \frac{i.(1+i)^N}{(1+i)^N - 1} \qquad (10)$$

The letter i in the above equation refers to the interest rate per year and is assumed a value of 5%, and the letter N is the plant lifetime in years and is assumed 20 years. To fit the original capital cost of equipment to the present time, the chemical engineering plant cost index [25] is utilized to convert the original cycle unit capital cost to reflect the year 2020 cost of that equipment. The following relationship is utilized for the fit:

$$Z_{k,Present} = Z_{k,original}\left(\frac{PCI_{Present}}{PCI_{original}}\right) \qquad (11)$$

Where $PCI_{Present}$ is the cost value at the present time and awarded a value of 567.5 and $PCI_{original}$ is the equipment cost value equation at the original time. The capital cost of a cycle unit, Z_k for the proposed hybrid cycle equipment is shown in Table 6 [26, 27].

Table 6: Capital cost equations for the proposed hybrid units

Unit	Capital Cost of Unit (Z_k), ($)	Ref.
ASU	$Z_{ASU,ref}\left(\frac{\dot{m}_{air,ASU}}{\dot{m}_{air,ASU,ref}}\right)^{0.6}$ $Z_{ASU,ref} = \$\ 1.001 \times 10^8, \dot{m}_{air,ASU,ref} = 100\ (\frac{kg}{s})$	[28]
Comb	$\left(\frac{46.08\dot{m}_{10}}{0.995 - P_1/P_{10}}\right)(1 + \exp(0.018T_1 - 26.4))$	[29]
CSP HX	$309.14\left(A_{CSP\ HX}^{0.85}\right)$	[30]
Turb	$479.34\left(\frac{\dot{m}_1}{0.92 - \eta_{turb}}\right) ln(P_1/P_2)\,[1 + exp(0.036T_1 - 54.4)]$	[31]
Rec	$2681\left(A_{recup}^{0.59}\right)$	[32]
Cl-I	$2143(A_{cooler\ I}^{0.514})$	[32]
C-I	$71.1\left(\frac{\dot{m}_5}{0.92 - \eta_{comp\ I}}\right)[(PR)(ln(PR)]$	[31]
IC	$2143(A_{intercooler}^{0.514})$	[32]
C-II	$71.1\left(\frac{\dot{m}_6}{0.92 - \eta_{comp\ II}}\right)[(PR)(ln(PR)]$	[31]
Cl-II	$2143(A_{cooler\ II}^{0.514})$	[32]
Pump	$32 \times 0.435\ \dot{m}_8{}^{0.55}\Delta P^{0.55}\left(\frac{\eta_{pump}}{\eta_{pump}-1}\right)^{1.05}$	[33]

Table 7: Exergy cost balance for the CSP configuration

Unit	Exergy Cost Rate Balance	Auxiliary Equation
CSP HX	$\dot{C}_1 = \dot{C}_{10} + \dot{C}_{molten\ salt} + \dot{Z}_{CSP\ HX}$	$c_{molten\ salt} = 14.986\ (\frac{\$}{GJ})$ [34]
Turb	$\dot{C}_2 + \dot{C}_{W_{turb}} = \dot{C}_1 + \dot{Z}_{turb}$	$c_1 = c_2$
Rec	$\dot{C}_{10} + \dot{C}_3 = \dot{C}_2 + \dot{C}_9 + \dot{Z}_{recup}$	$c_3 = c_2$
Cl-I	$\dot{C}_4 + \dot{C}_{16} = \dot{C}_3 + \dot{C}_{15} + \dot{Z}_{cooler\ I}$	$c_3 = c_4$
C-I	$\dot{C}_5 = \dot{C}_4 + \dot{C}_{W_{comp\ I}} + \dot{Z}_{comp\ I}$	$c_{w,comp\ I} = c_{w,turb}$
IC	$\dot{C}_6 + \dot{C}_{14} = \dot{C}_5 + \dot{C}_{13} + \dot{Z}_{intercooler}$	$c_5 = c_6$
C-II	$\dot{C}_7 = \dot{C}_6 + \dot{C}_{W_{comp\ II}} + \dot{Z}_{comp\ II}$	$c_{w,comp\ II} = c_{w,turb}$
Cl-II	$\dot{C}_8 + \dot{C}_{12} = \dot{C}_7 + \dot{C}_{11} + \dot{Z}_{cooler\ II}$	$c_7 = c_8$
Pump	$\dot{C}_9 = \dot{C}_8 + \dot{C}_{W_{Pump}} + \dot{Z}_{Pump}$	$c_{w,pump} = c_{w,turb}$

The total capital cost in ($) is calculated by:

$$Z_{total} = \sum_{k=1}^{n} Z_k\ , n = total\ number\ of\ equipment \qquad (12)$$

Applying equation (7) to all cycle units and their supplementary auxiliary equations leads to the formation of a system of linear equations representing the whole cycle, mathematically. To successfully solve the system's mathematical representation, the number of equations and unknowns must be equal. However, the number of unknowns is larger than the number of equations at this stage. Hence, auxiliary equations are utilized to bridge the gap between the number of equations and unknowns for the system in hand. Tables 7 and 8 show the system's cost balance equations and their subsequent auxiliary equations for both configurations. The product stream cost rate of the cycle is calculated utilizing the specific exergy costing (SPECO) approach [35].

Table 8: Exergy cost balance for the OC configuration

Cycle Unit	Exergy Cost Rate Balance	Auxiliary Equation
ASU	$\dot{C}_{19} + \dot{C}_{20} = \dot{C}_{18} + \dot{C}_{W_{ASU}} + \dot{Z}_{ASU}$	$c_{w,ASU} = c_{w,turb}$ $\dot{C}_{19} = 0.2658\ \dot{C}_{20}$
Comb	$\dot{C}_1 = \dot{C}_{10} + \dot{C}_{17} + \dot{C}_{19} + \dot{Z}_{comb}$	---
Turb	$\dot{C}_2 + \dot{C}_{W_{turb}} = \dot{C}_1 + \dot{Z}_{turb}$	$c_1 = c_2$
Rec	$\dot{C}_3 + \dot{C}_{10} + \dot{C}_{21} = \dot{C}_2 + \dot{C}_{9a} + \dot{C}_{20} + \dot{Z}_{recup}$	$c_3 = c_2$ $c_{20} = c_{21}$
Cl-I	$\dot{C}_4 + \dot{C}_{16} = \dot{C}_3 + \dot{C}_{15} + \dot{Z}_{cooler\ I}$	$c_3 = c_4$
C-I	$\dot{C}_5 = \dot{C}_{4a} + \dot{C}_{W_{comp\ I}} + \dot{Z}_{comp\ I}$	$c_{w,comp\ I} = c_{w,turb}$
IC	$\dot{C}_6 + \dot{C}_{14} = \dot{C}_5 + \dot{C}_{13} + \dot{Z}_{intercooler}$	$c_5 = c_6$
C-II	$\dot{C}_7 = \dot{C}_6 + \dot{C}_{W_{Comp\ II}} + \dot{Z}_{comp\ II}$	$c_{w,comp\ II} = c_{w,turb}$
Cl-II	$\dot{C}_8 + \dot{C}_{12} = \dot{C}_7 + \dot{C}_{11} + \dot{Z}_{cooler\ II}$	$c_7 = c_8$
Pump	$\dot{C}_9 = \dot{C}_8 + \dot{C}_{W_{Pump}} + \dot{Z}_{Pump}$	$c_{w,pump} = c_{w,turb}$
SP-I	$\dot{C}_9 = \dot{C}_{9a} + \dot{C}_{9b}$	$\dot{C}_{9a} = (\frac{\dot{m}_{Rec,CO_2}}{\dot{m}_{CO_2}})\ \dot{C}_9$
SP-II	$\dot{C}_4 = \dot{C}_{4a} + \dot{C}_{4b}$	$\dot{C}_{4a} = (\frac{\dot{m}_{Exp,CO_2}}{\dot{m}_{total}})\ \dot{C}_4$

For the OC configuration, the unit cost of the natural gas (c_f) is \$3 per GJ of fuel. Assuming an escalation rate of r_n= 6% for the first quarter of operation [29], the levelized cost rate of stream 17 (fuel) supplied to the combustion chamber is calculated as:

$$\dot{C}_{17} = 3600 \times \dot{n}_f c_f \overline{LHV} N_h (1+r_n)^5 CRF \times \frac{k_f(1-k_f^{nt})}{1-k_f} \quad ;\ k_f = \frac{1+r_n}{1+i} \qquad (13)$$

Where $\dot{n}_f$ is the mole flowrate of fuel (kmol/h) and N_h is the annual operational availability of the plant in $(h/year)$. The average fuel lower heating value ($\overline{\text{LHV}}$) in the above equation is 802,361 kJ/kmol.

D. HYBRID CYCLE PERFORMANCE PARAMETERS ANALYSIS

Sound performance measurement requires to assign specific criteria of performance. Hence, exergy efficiency (η_{ex}), energy efficiency (η_{th}) and total product unit cost ($c_{p,total}$) are employed to perform the hybrid cycle performance in this study. The energy efficiency, according to the first law of thermodynamics, is the ratio of useful output energy to the input energy of the cycle and is determined as:

$$\eta_{th} = \frac{\dot{W}_{net}}{\dot{Q}_{in}} \qquad (14)$$

The exergy efficiency, according to the second law of thermodynamics, is calculated as [20]:

$$\eta_{ex} = \frac{\dot{E}_{Product}}{\dot{E}_{Fuel}} = 1 - \frac{\dot{E}_{D,total}}{\dot{E}_{Fuel}} \qquad (15)$$

Where $\dot{E}_{D,total}$ is the sum of all exergy destructed in all cycle units.

The total product unit is calculated by [24]:

$$c_{p,total} = \frac{\sum_{k=1}^{NK} \dot{Z}_{k,i} + \sum_{i=1}^{NF} \dot{C}_{Fuel,i}}{\sum_{i=1}^{NP} \dot{E}_{Product,i}} \qquad (16)$$

Where $\dot{C}_{Fuel}$ is the fuel exergy stream cost and $\dot{E}_{Product}$ is the product exergy stream. NK is the number of the cycle units, NF is the number of fuels to the cycle, and NP is the number of products of the cycle. The levelized cost of electricity ($LCOE$) in (\$/kWh) is calculated by dividing the total capital investment cost of the cycle units and the cost of fuel input by the net power produced from the hybrid cycle [36]:

$$LCOE = \frac{\sum_{i=1}^{k} \dot{Z}_k + \dot{C}_{Fuel}}{\dot{W}_{net}} \qquad (17)$$

The average cost per unit exergy of fuel in (\$/GJ) is calculated by [20]:

$$c_{F,k} = \dot{C}_{F,k} / \dot{E}_{F,k} \qquad (18)$$

The cost rate of exergy destruction in (\$/h) is calculated by [20]:

$$\dot{C}_{D,k} = c_{F,k} . \dot{E}_{D,k} \qquad (19)$$

The cost rate of exergy loss in (\$/h) is calculated by [20]:

$$\dot{C}_{L,k} = c_{F,k} . \dot{E}_{L,k} \qquad (20)$$

The exergoeconomic factor is calculated by [20]:

$$f_k = \dot{Z}_k / (\dot{Z}_k + \dot{C}_{D,k} + \dot{C}_{L,k}) \qquad (21)$$

The relative cost difference (r_k) is calculated by [20]:

$$r_k = \frac{1-\epsilon_k}{\epsilon_k} + \frac{\dot{Z}_k}{c_{F,k}\dot{E}_{P,k}} \qquad (22)$$

The energy, exergy, and exergoeconomic equations representing the hybrid cycle are modeled using the EES software.

RESULTS AND DISCUSSION

To analyze the impact of the main cycle thermodynamic parameters, a parametric study is performed, and its results are analyzed. The hybrid's model design input parameters for the base case of the CSP and OC standalone configurations are presented in Table 9. The inlet parameters apply for both cycle configurations.

Table 9: Model main input parameters

Parameter	Value
Dead state temperature (°C)	25
Dead state pressure (bar)	1
Turbine isentropic efficiency (%)	90
Turbine inlet temperature (°C)	700
Turbine inlet pressure (bar)	300
Turbine pressure ratio (--)	10
Turbine inlet mass flowrate (kg/s)	125
Minimum compressor inlet temperature (°C)	20
Compressor inlet pressure (bar)	28.8
Compressor pressure ratio (--)	2.78
Compressor isentropic efficiency (%)	85
Pump isentropic efficiency (%)	80
Fractional pressure drop (%)	2
Cooler pinch point temperature (°C)	5

A. EXERGY AND EXERGOECONOMIC ANALYSIS

The main model output performance parameters are presented in Table 10 for CSP configurations and Table 11 for the OC configuration. A comparison between the two standalone configurations reveals that the produced net power output for both configurations is approximately the same at 30 MW. Although the second law of thermodynamics efficiency is within the same range, in terms of the first law of thermodynamics efficiency, the OC configuration is higher by 7%. The total unit product cost ($/GJ) for the CSP standalone configuration is approximately twice that of the OC configuration. This means that fossil fuel combustion is less expensive than providing heat through solar energy. It is worth mentioning that the combustion chamber and the ASU supply the OC configuration heat, while heat supplied to the CSP configuration is provided by the CSP plant. The CSP plant is much more complicated and hence costs more. Finally, the unit cost of electricity in units of (Cent/kWh) is 9.8 for the CSP standalone configuration and 6.1 for the OC configuration.

The steady-state operations thermodynamic parameters of the base case for both configurations are displayed in Figure 6 and Figure 7 of Annex B. In addition to temperature, the mass, exergy, and cost flow rates of the cycle units are shown in both figures.

In exergoeconomic evaluation of thermal systems, certain quantities known as the thermo-economic variables play a vital role and give insight on the optimization potential. Such variables are useful for applications in existing power plants, as they help identify improvements realized by increasing or decreasing the unit exergy cost. They also pinpoint the exergy destruction locations in the system under examination. These variables are the cost rate of exergy destruction ($\dot{C}_{D,k}$), relative cost difference (r_k) and exergoeconomic factor (f_k). The costs associated with exergy destruction and losses in a component are hidden costs and can be revealed only using exergoeconomic analysis.

Table 10: Model main output parameters for CSP configuration

Parameter	Value
Net power (MW)	29.52
First law efficiency (%)	40.55
Second law efficiency (%)	56.92
Total unit product cost ($/GJ)	27.55
Unit cost of electricity (Cent/kWh)	9.8

Table 11: Model main output parameters for OC configuration

Parameter	Value
Net power (MW)	30.73
First law efficiency (%)	47.38
Second law efficiency (%)	54.72
Total unit product cost ($/GJ)	12.98
Unit cost of electricity (Cent/kWh)	6.1

A cycle unit with a high value of $\dot{C}_{D,k} + \dot{Z}_k$ means that this unit is important and more attention towards it is recommended. The exergoeconomic factor is the contribution of non-exergy related cost to the total cost of the system units and is used to identify units with a significant cost. A low value of f_k for a unit suggests that cost savings for the entire system might be achieved by improving this unit's efficiency. This means reducing exergy destruction is essential, even if it means that this unit's capital and operating cost increases. While a higher value of f_k suggests a decrease in the unit's capital cost is beneficial even if at the expense of exergetic efficiency. The relative cost difference (r_k) for a unit represents the average cost per unit exergy between fuel and product, and it is useful to evaluate and optimize a system unit [29]

Table 12 and Table 13 show the results obtained from the exergoeconomic analysis of the proposed CSP and OC standalone configurations, respectively. The two tables summarize the base case values of exergy destruction, exergy efficiency, and exergoeconomic parameters of both configurations' major units. For the CSP case, it shows that the main CSP heat exchanger has the highest value of $\dot{C}_{D,k} + \dot{Z}_k$ along with the lowest value of f_k compared to other units, and then it is followed by the CSP recuperator. This is attributed to the high irreversibility arising from the high temperature difference existing in these units. Therefore, the two units are considered the most critical components from the thermo-economic perspective for the CSP configuration. The low value of f_k for the unit shows that the exergy destruction dominates the

cost associated with this unit while the remaining part is caused by the $\dot{Z}_k$ value. So, it can be concluded that reducing the exergy destruction in the CSP main heat exchanger and the recuperator units could be cost-effective for the entire cycle, even if it increases the unit investment costs. Therefore, for exergoeconomic performance enhancement, using a recuperator with higher efficiency is recommended.

For the OC configuration, the highest value of $\dot{C}_{D,k} + \dot{Z}_k$ and the lowest value of f_k belongs to the combustor with exergetic efficiency of 76%. The ASU has the second highest $\dot{C}_{D,k} + \dot{Z}_k$ value. Therefore, replacing the ASU with a lower purchasing cost unit is recommended for an overall exergoeconomic performance enhancement for this configuration.

Table 12: Results of the exergoeconomic analysis for the base case of CSP configuration

Cycle Unit	ϵ_k (%)	$\dot{C}_{D,k}$ ($/h)	$\dot{Z}_k$ ($/h)	$\dot{C}_{D,k} + \dot{Z}_k$ ($/h)	r_k (%)	f_k (%)
CSP HX	90.46	669.9	0.3083	670.2	10.55	0.046
Turb	95.33	164.6	71.61	236.21	7.029	30.32
Rec	62.05	589.7	0.3977	590.1	8.078	0.067
Cl-I	96.11	75.93	0.941	76.87	1.61	1.224
C-I	87.56	24.47	5.818	30.29	18.12	19.21
IC	96.56	76.01	1.081	77.1	1.465	1.402
C-II	90.71	20.79	4.569	25.36	11.72	18.02
Cl-II	94.26	138.9	1.181	140.1	1.971	0.844
Pump	76.63	85.92	2.198	88.11	3.427	2.949

Table 13: Results of the exergoeconomic analysis for the base case of OC configuration

Cycle Unit	ϵ_k (%)	$\dot{C}_{D,k}$ ($/h)	$\dot{Z}_k$ ($/h)	$\dot{C}_{D,k} + \dot{Z}_k$ ($/h)	r_k (%)	f_k (%)
Comb	76.48	1076	3.947	1079.95	30.87	0.3655
Turb	97.38	119.9	69.99	189.9	8.791	36.86
Rec	95.21	222.7	0.5323	223.2	14.39	0.2384
Cl-I	96.4	43.2	0.9684	44.17	1.473	2.192
C-I	89.53	19.31	4.535	23.85	20.35	19.01
IC	96.57	45.9	1.066	46.9	1.475	2.271
C- II	91.82	17.25	4.025	21.28	14.58	18.91
Cl-II	94.19	85.47	1.164	86.63	2.032	1.344
Pump	77.3	50.8	2.17	52.9	3.373	4.097
ASU	93.93	69.98	572.5	642.5	60.1	89.25

B. PARAMETRIC ANALYSIS

The influence of specific thermodynamic parameters on the cycle performance is important. Therefore, energetic, exergetic, and economic parametric analysis is performed for such parameters. The parametric study is conducted under variable operating conditions while keeping all other parameters unchanged based on the mentioned assumptions and values provided in Table 6. The thermodynamic parameters considered for this study are the turbine's inlet pressure (P_1), the turbine's inlet temperature (T_1), the turbine's outlet pressure (P_2). On the other hand, the performance parameters selected to assess the proposed system are the exergy efficiency and the levelized cost of electricity.

Figure 8a and Figure 8b of Annex C demonstrate the effect of the turbine inlet pressure on the proposed CSP and OC configurations' performance, respectively. Since the circulating mass flow rate of CO_2 is kept constant, the net power delivered for both configurations increases with η_{ex}. These results indicate that increasing T_1 is conducive to improving the thermodynamic and exergoeconomic performances of both configurations. It is worth mentioning that the increment of the net produced power is dominant compared with the increase in the capital installment cost, which in turn lowers the LCOE with the increase in the turbine inlet temperature. The total capital installment and maintenance cost of the two configurations (Z_{tot}) decreases with the rise in T_1 due to the decrements of the Z_k values of the turbine, compressors, and the recuperator units, which account for the main portion of Z_{tot}. Also, fuel cost ($\dot{C}_{molten\ salt}$) keeps constant when T_1 changes. In addition, the $c_{p,total}$ decreases with an increasing T_1.

Similar trends were obtained when the turbine inlet pressure is increased from 24 MPa to 36 MPa for both configurations, as presented in Figure 9 of Annex C. It is known that the compressor's power consumption is dominant in comparison with that of the pump. Therefore, the net power output (W_{net}) is mainly related to the compressors' power consumption and the turbine's output power. Due to a constant turbine outlet pressure, both the turbine's output power and the compressors' power consumption increase with increased turbine inlet pressure. Note that the CSP main heat exchanger's outlet temperature is kept constant (700°C) as P_1 increases. W_{net} of both configurations increases with P_1 when the increment of the turbine's output work is larger than that of the compressors; otherwise, W_{net} decreases.

As shown in Figure 10 of Annex C, the increase in net power decreases LCOE for both configurations. In addition, for both configurations, the decrease in the turbine's outlet pressure reduces both turbine's produced power and compressor's power consumption. For the CSP configuration, the reduction in P_2 results in a decrease in the capital and operating cost, leading to a decrease in LCOE. Unfortunately, this is not the case for the OC configuration. As P_2 increases, LCOE first decreases and then increases. However, the same P_2 increase keeps the exergy efficiency constant at first before causing it to decrease. This indicates that there is an optimum turbine outlet pressure with which the total unit product cost is minimized for this particular configuration. The increase in the LCOE is attributed to the increase in the combustor, ASU, and recuperator capital installment cost, which is dominant in determining the total capital installment and maintenance cost of the OC configuration.

CONCLUSION

Although both configurations obtained similar power output and exergy efficiency, the thermal efficiency was higher for the OC configuration. The total product cost in ($/GJ) for the OC

was half of that for the CSP. The unit cost of electricity in (Cent/kWh) for the CSP standalone configuration is approximately 60% higher than that of the OC configuration.

In the CSP configuration, the main heat exchanger and the recuperator are the most significant units to consider for savings. Therefore, reducing the exergy destruction in the CSP main heat exchanger and the recuperator units could be cost-effective for the entire cycle, even if this would increase the component investment costs. Therefore, for exergoeconomic performance enhancement, using a recuperator with higher efficiency is recommended. On the other hand, for the OC configuration, the combustor and ASU are the most critical units to consider for savings. Therefore, a replacement for the ASU unit with a lower purchasing cost is recommended for overall exergoeconomic performance enhancement.

The parametric study results showed that increasing the turbine's inlet temperature is conducive to improving both configurations' thermodynamic and exergoeconomic performances. Similar trends were also obtained for the turbine inlet pressure for both configurations.

Future work includes conducting an optimization study on the proposed hybrid cycle. Also, conducting another exergoeconomic analysis while the proposed hybrid is powered simultaneously by CSP and OC heat sources is considered for the next research topic.

NOMENCLATURE

c_f	Unit cost of the natural gas [$/GJ]
$c_{F,k}$	Average cost per unit exergy of fuel for the k[th] component [$/GJ]
c_k	Cost per unit exergy for the k[th] component [$/GJ]
$\dot{C}_{D,k}$	Cost rate of exergy destruction for the k[th] component [$/h]
$\dot{C}_{e,k}$	Cost rate associated with the outlet streams of a unit for the k[th] component [$/h]
$\dot{C}_{i,k}$	Cost rate associated with the inlet streams of a unit for the k[th] component [$/h]
$\dot{C}_{L,k}$	Cost rate associated with exergy loss for k[th] component [$/hr]
$\dot{C}_{q,k}$	Cost rate associated with thermal energy for the k[th] component [$/h]
$\dot{C}_{w,k}$	Cost rate associated with power for the k[th] component [$/h]
$c_{p,total}$	Total unit cost of the product [$/GJ]
$\dot{E}_D$	Exergy destruction [W]
E_e	Exergy of the exit [W]
E_i	Exergy of the inlet [W]
$\dot{E}_{Fuel,CSP}$	Exergy of the fuel for the CSP configuration [W]
$\dot{E}_{Fuel,i}$	Exergy of the fuel for the i[th] component [W]
$\dot{E}_{Fuel,OC}$	Exergy of the fuel for the CSP configuration [W]
$\dot{E}_{Product,i}$	Exergy of the product for the i[th] component [W]
f_k	Exergoeconomic factor for the k[th] component
h_i	Enthalpy at the inlet [J/Kg CO_2]
h_{out}	Enthalpy at the Outlet [J/Kg CO_2]
ho	Enthalpy at the Outlet [J/Kg CO2]
k_f	Exergoeconomic factor for the kth component
MW_{CH_4}	Molecular weight of methane
$\dot{m}e$	Mass flowrate at the exit [Kg/s]
$\dot{m}I$	Mass flowrate at the inlet [Kg/s]
$\dot{n}_f$	Mole flowrate of fuel [kmol/h]
N_h	The annual operational availability of the plant $[h/year]$
$PCI_{original}$	Equipment cost value at the original time
$PCI_{Present}$	Equipment cost value at the present time
$\dot{Q}_{CSP}$	Heat transfer supplied by CSP main heat exchanger [W]
$\dot{Q}_i$	Heat transfer for the i[th] component [W]
$\dot{Q}_{in}$	Heat input [W]
r_k	Relative cost difference
r_n	Escalation rate
T_s	Heat source temperature [K]
T_0	Dead state temperatures [K]
$\dot{W}$	Work [W]
W_{net}	Network [W]
Z_k	Capital cost of a cycle unit for the k[th] component [$]
$Z_{present}$	Capital cost of a cycle unit at the present time [$]
$Z_{original}$	Capital cost of a cycle unit at the original time [$]
Z_{total}	Total capital cost [$]
$\dot{Z}_k$ ($/h)	Capital, operational, and maintenance cost rate for the k[th] component [$/h]
ϵ_k	Efficiency according to the second law of thermodynamics for the kth component
η_{ex}	Exergy efficiency
η_{th}	Energy efficiency according to the first law of thermodynamics
μ	Chemical potential
τ	The annual operational availability of the plant [h/year]
φ	The plant maintenance factor

REFERENCES

1. Administration, U.E.I., *Annual energy outlook 2018 with projections to 2050.* 2018.
2. Syblik, J., et al., *Analysis of supercritical CO2 Brayton power cycles in nuclear and fusion energy.* Fusion Engineering and Design, 2019. 146: p. 1520-1523.
3. Kacludis, A., et al., *Waste heat to power (WH2P) applications using a supercritical CO2-based power cycle*, in *Power-Gen International*. 2012. p. 11-13.
4. Brun, K., P. Friedman, and R. Dennis, *Fundamentals and applications of supercritical carbon dioxide (sCO2) based power cycles*. 2017: Woodhead publishing.
5. Allam, R., et al., *Demonstration of the Allam Cycle: an update on the development status of a high efficiency supercritical carbon dioxide power process employing full carbon capture.* Energy Procedia, 2017. 114: p. 5948-5966.
6. Castle, W., *Air separation and liquefaction: recent developments and prospects for the beginning of the new*

millennium. International Journal of Refrigeration, 2002. 25(1): p. 158-172.
7. Allam, R., et al., *High efficiency and low cost of electricity generation from fossil fuels while eliminating atmospheric emissions, including carbon dioxide.* Energy Procedia, 2013. 37: p. 1135-1149.
8. Allam, R.J., M. Palmer, and G.W. Brown, *System and method for high efficiency power generation using a carbon dioxide circulating working fluid*. 2013, Google Patents.
9. Barba, F.C., et al., *A technical evaluation, performance analysis and risk assessment of multiple novel oxy-turbine power cycles with complete CO2 capture.* Journal of cleaner production, 2016. 133: p. 971-985.
10. Allam, R., et al. *The oxy-fuel, supercritical CO2 Allam Cycle: New cycle developments to produce even lower-cost electricity from fossil fuels without atmospheric emissions*. in *ASME Turbo Expo 2014: Turbine Technical Conference and Exposition*. 2014. American Society of Mechanical Engineers.
11. Demirbas, A., *Recent advances in biomass conversion technologies.* Energy Edu Sci Technol, 2000. 6: p. 19-41.
12. Panwar, N., S. Kaushik, and S. Kothari, *Role of renewable energy sources in environmental protection: a review.* Renewable Sustainable Energy Reviews, 2011. 15(3): p. 1513-1524.
13. Ordorica-Garcia, G., A.V. Delgado, and A.F. Garcia, *Novel integration options of concentrating solar thermal technology with fossil-fuelled and CO2 capture processes.* Energy Procedia, 2011. 4: p. 809-816.
14. Barlev, D., R. Vidu, and P. Stroeve, *Innovation in concentrated solar power.* Solar energy materials and solar cells, 2011. 95(10): p. 2703-2725.
15. Mehos, M., et al., *Concentrating solar power Gen3 demonstration roadmap*. 2017: National Renewable Energy Laboratory , Golden, Colorado, USA.
16. Louis, A.T. and T. Neises. *Analysis and Optimization for Off-Design performance of the recompression s-CO2 cycles for high temperature CSP applications*. in *The 5th International Symposium-Supercritical CO2 Power Cycles*. 2016.
17. Peterseim, J.H., et al., *Concentrating solar power hybrid plants–enabling cost effective synergies.* Renewable energy, 2014. 67: p. 178-185.
18. Alenezi, A. and J.S. Kapat. *Thermodynamic Analysis of sCO2 Allam Cycle for Concentrated Solar Power Complemented with Oxy-Combustion*. in *AIAA Propulsion and Energy 2019 Forum*. 2019.
19. Sharqawy, M.H. and S.M. Zubair, *On exergy calculations of seawater with applications in desalination systems.* International Journal of Thermal Sciences, 2011. 50(2): p. 187-196.
20. Bejan, A., G. Tsatsaronis, and M.J. Moran, *Thermal design and optimization*. 1995: John Wiley & Sons.
21. El-Halwagi, M.M., *Sustainable design through process integration: fundamentals and applications to industrial pollution prevention, resource conservation, and profitability enhancement*. 2017: Butterworth-Heinemann.
22. Sayyaadi, H. and A. Saffari, *Thermoeconomic optimization of multi effect distillation desalination systems.* Applied Energy, 2010. 87(4): p. 1122-1133.
23. Alharbi, S., M.L. Elsayed, and L. Chow. *Thermo-Economic Analysis of an Integrated Supercritical CO2 Brayton Cycle and Multiple Effect Desalination Systems*. in *ASME 2018 International Mechanical Engineering Congress and Exposition*. 2018. American Society of Mechanical Engineers.
24. Vieira, L.S., J.L. Donatelli, and M.E. Cruz, *Exergoeconomic improvement of a complex cogeneration system integrated with a professional process simulator.* Energy Conversion and Management, 2009. 50(8): p. 1955-1967.
25. Ozcan, H. and I. Dincer, *Exergoeconomic optimization of a new four-step magnesium–chlorine cycle.* international journal of hydrogen energy, 2017. 42(4): p. 2435-2445.
26. Marchionni, M., G. Bianchi, and S.A. Tassou, *Techno-economic assessment of Joule-Brayton cycle architectures for heat to power conversion from high-grade heat sources using CO2 in the supercritical state.* Energy, 2018. 148: p. 1140-1152.
27. Alharbi, S., M.L. Elsayed, and L.C. Chow, *Exergoeconomic analysis and optimization of an integrated system of supercritical CO2 Brayton cycle and multi-effect desalination.* Energy, 2020: p. 117225.
28. Ebrahimi, A., et al., *Energetic, exergetic and economic assessment of oxygen production from two columns cryogenic air separation unit.* Energy, 2015. 90: p. 1298-1316.
29. Bejan, A. and G. Tsatsaronis, *Thermal design and optimization*. 1996: John Wiley & Sons.
30. Schultz, K., et al., *Large-scale production of hydrogen by nuclear energy for the hydrogen economy*. 2003, GENERAL ATOMICS (US).
31. Ghaebi, H., et al., *Energy, exergy and thermoeconomic analysis of a combined cooling, heating and power (CCHP) system with gas turbine prime mover.* International Journal of Energy Research, 2011. 35(8): p. 697-709.
32. Guo-Yan, Z., W. En, and T. Shan-Tung, *Techno-economic study on compact heat exchangers.* International journal of energy research, 2008. 32(12): p. 1119-1127.
33. El-Sayed, Y., *Designing desalination systems for higher productivity.* Desalination, 2001. 134(1-3): p. 129-158.
34. Ma, Y., et al., *Optimal integration of recompression supercritical CO2 Brayton cycle with main compression intercooling in solar power tower system based on exergoeconomic approach.* Applied energy, 2019. 242: p. 1134-1154.
35. Lazzaretto, A. and G. Tsatsaronis, *SPECO: a systematic and general methodology for calculating efficiencies and costs in thermal systems.* Energy, 2006. 31(8-9): p. 1257-1289.
36. Nami, H., S. Mahmoudi, and A. Nemati, *Exergy, economic and environmental impact assessment and optimization of a novel cogeneration system including a gas turbine, a supercritical CO2 and an organic Rankine cycle (GT-HRSG/SCO2).* Applied Thermal Engineering, 2017. 110: p. 1315-1330.

ANNEX A

P-H DIAGRAMS FOR THE CSP AND OC STANDALONE CONFIGURATIONS

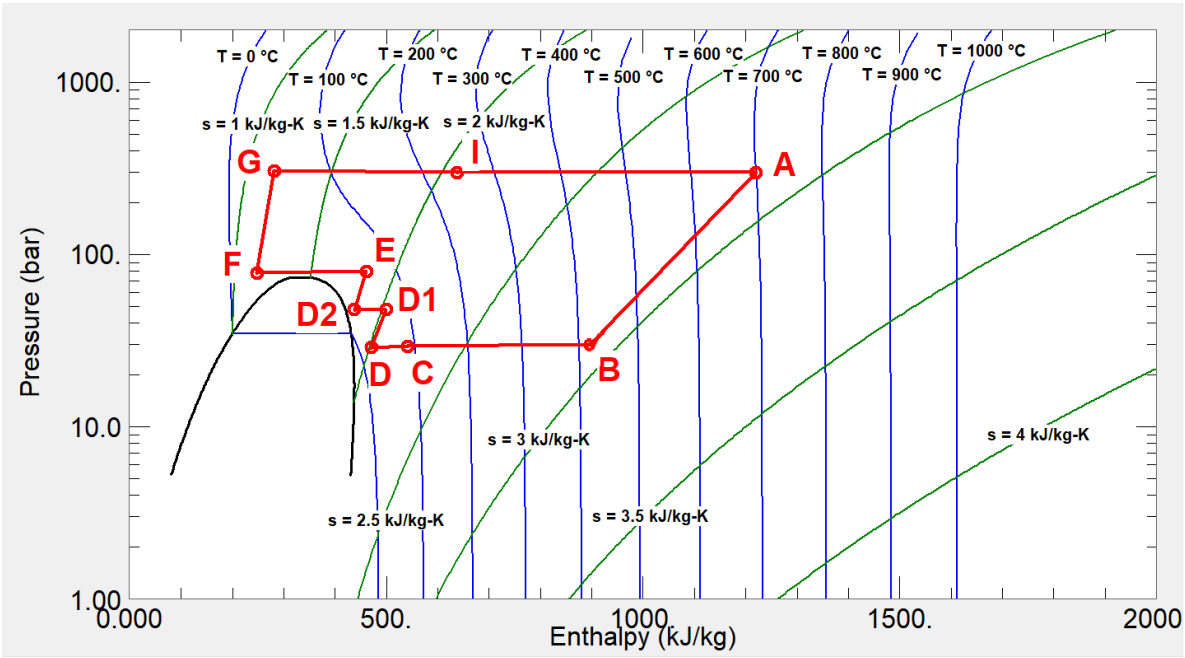

Figure 4: Pure CO_2 log P-h diagram of the CSP standalone configuration

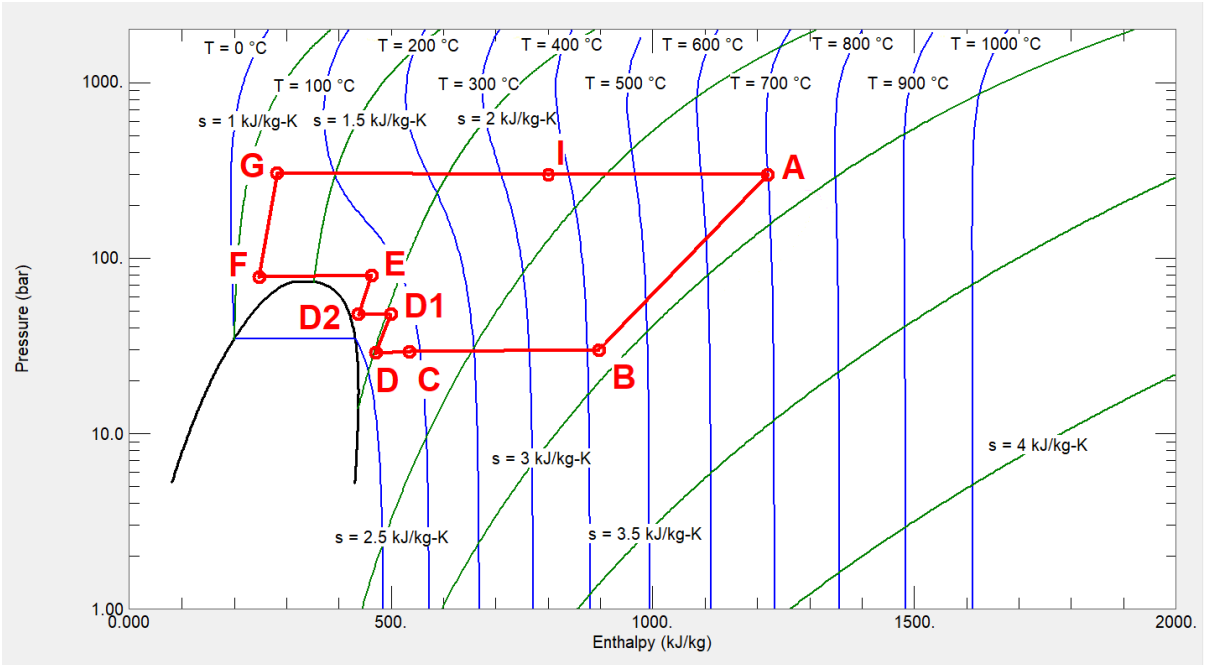

Figure 5: Pure CO_2 log P-h diagram of the OC standalone configuration

ANNEX B

STEADY STATE MASS, EXERGY, AND COST FLOWRATES FIGURES

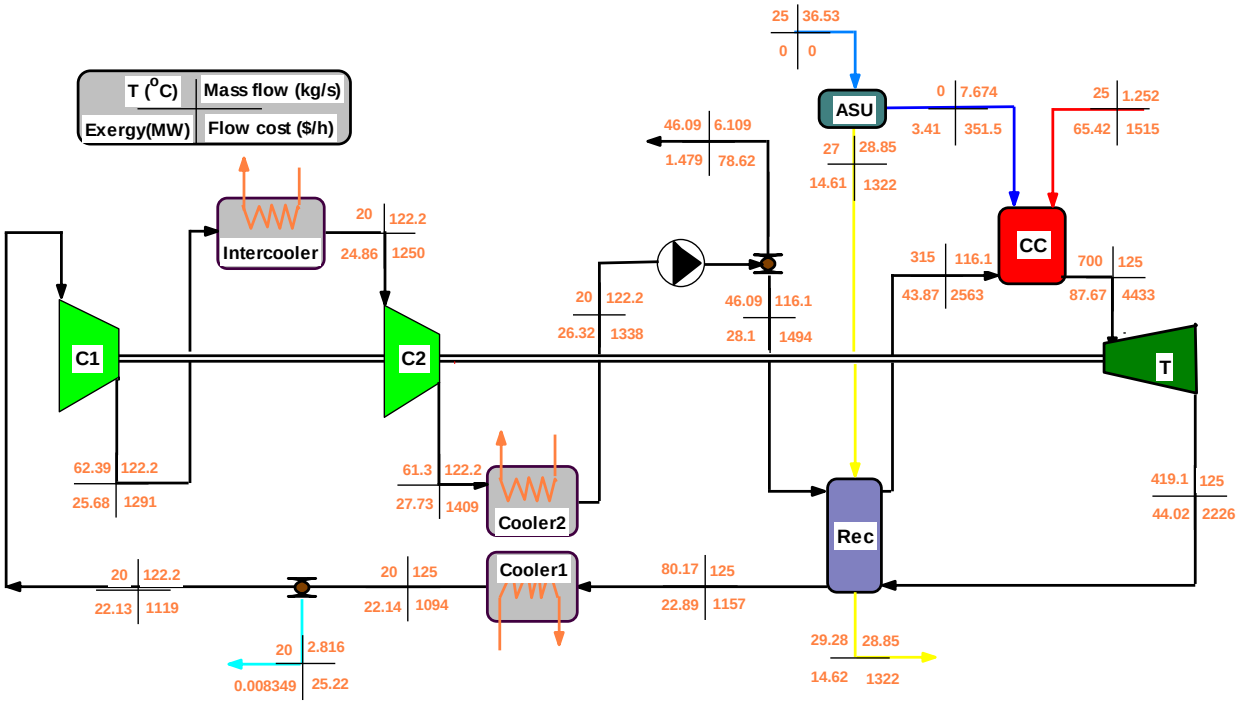

Figure 6: Mass, exergy, and cost flowrates of the hybrid cycle CSP standalone configuration

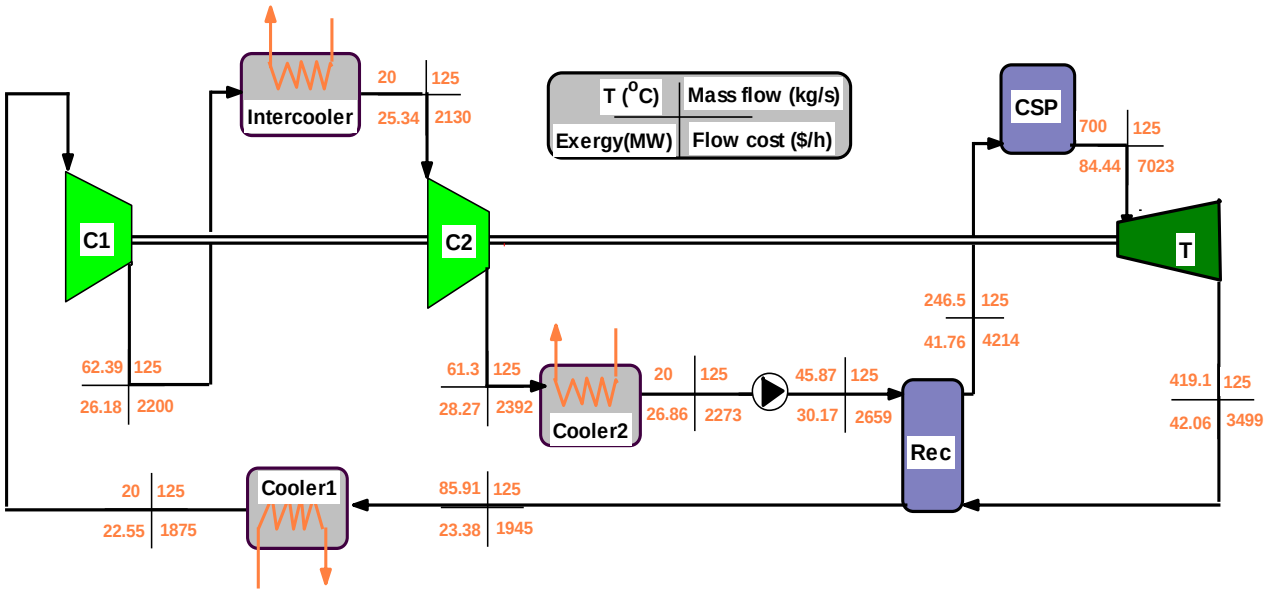

Figure 7: Mass, exergy, and cost flowrates of the hybrid cycle OC standalone configuration

ANNEX C:

PARAMETRIC STUDY FIGURES

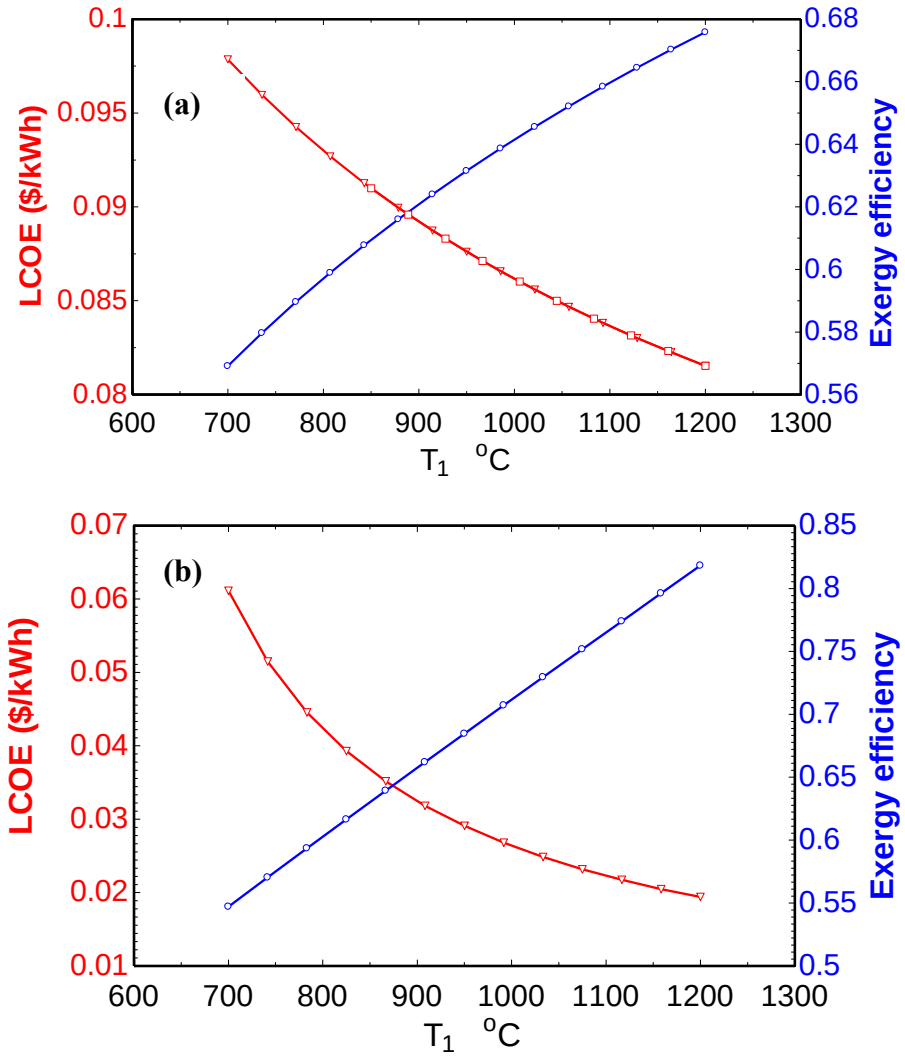

Figure 8: Variations of exergy efficiency and LCOE for (a) CSP and (b) OC configurations with turbine inlet temperature

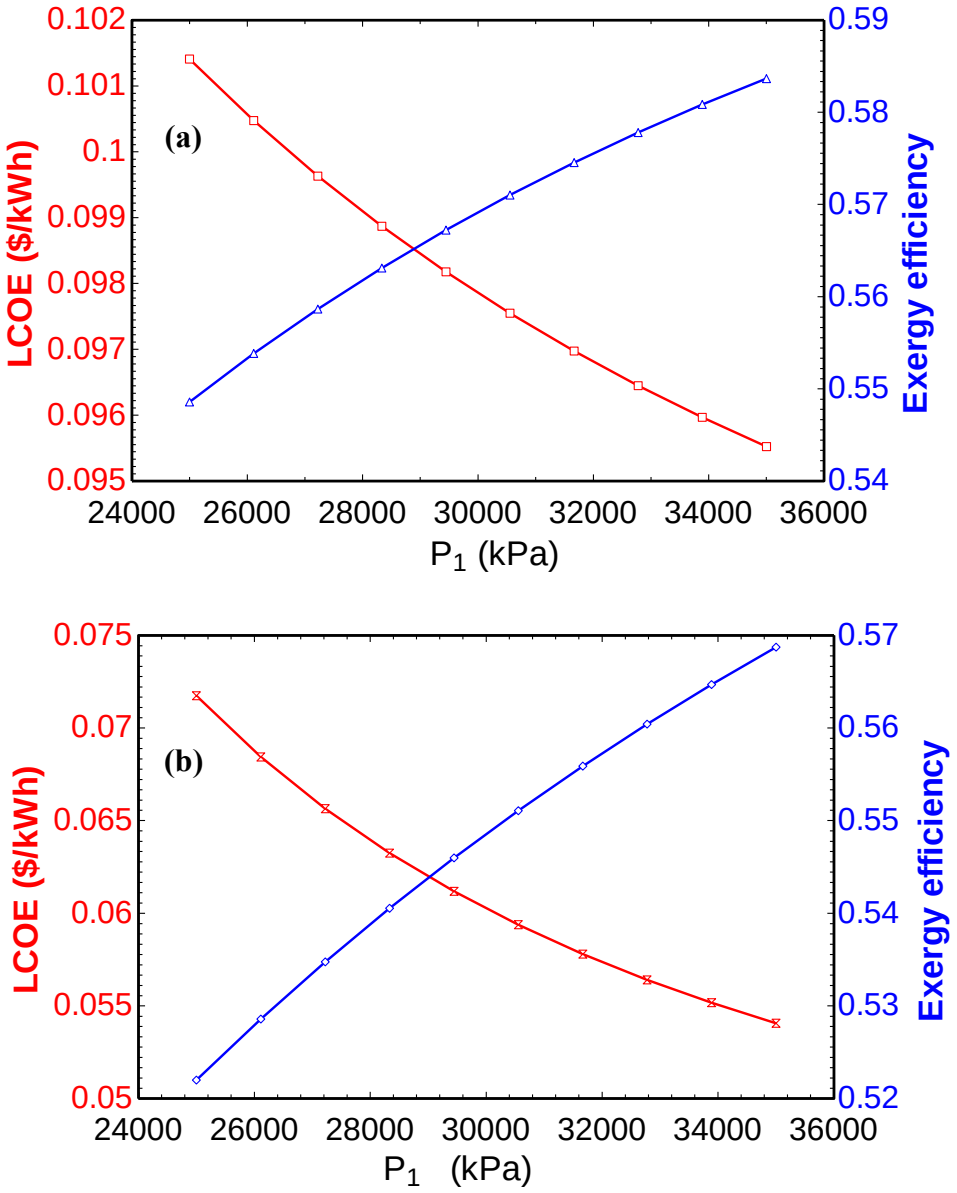

Figure 9: Variations of exergy efficiency and LCOE for (a) CSP and (b) OC configurations with turbine inlet pressure

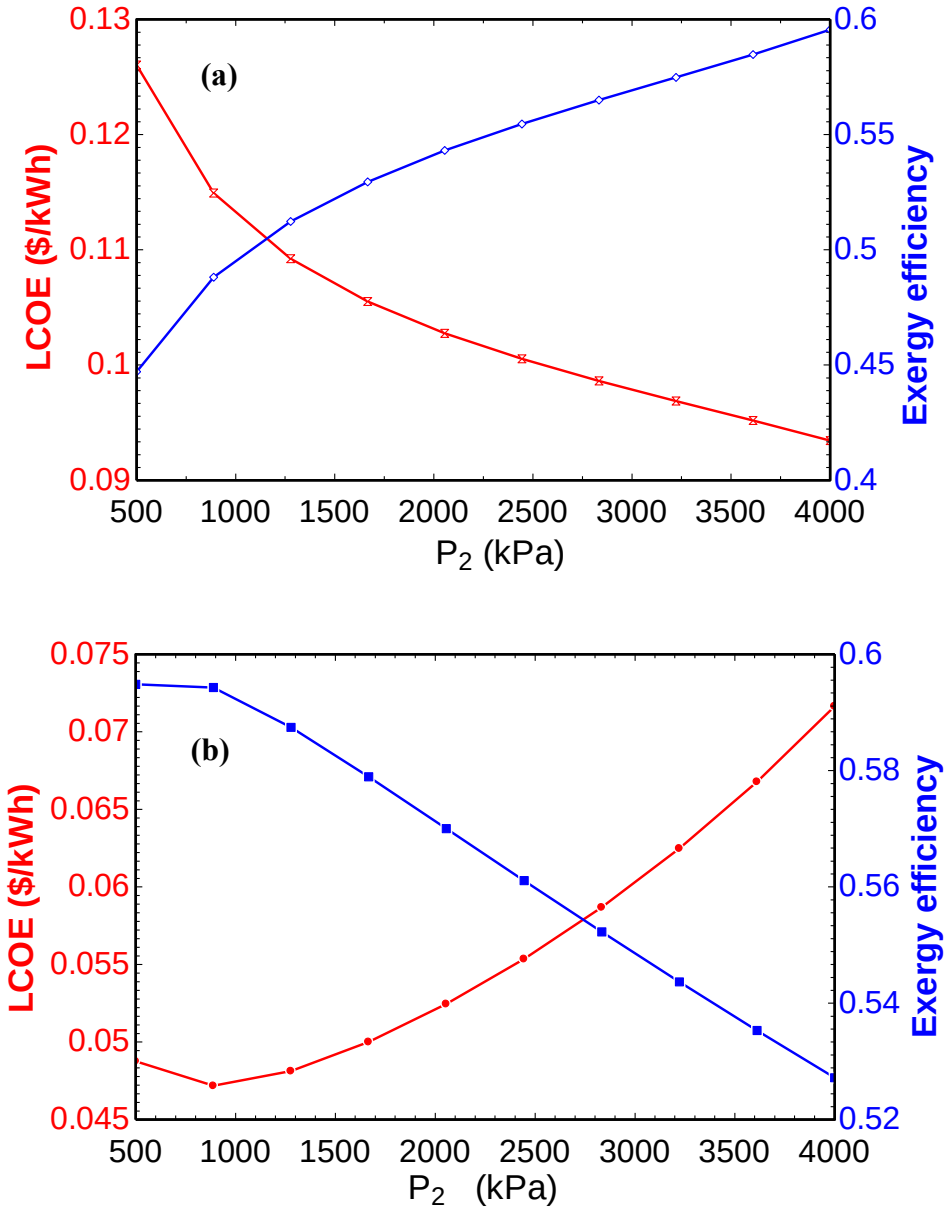

Figure 10: Variations of exergy efficiency and LCOE for (a) CSP and (b) OC configurations with turbine exit pressure

DOI: 10.17185/duepublico/73980
URN: urn:nbn:de:hbz:464-20210330-123551-1